Building Three-Dimensional Graphene Frameworks for Energy Storage and Catalysis

Minghao Yu, Yongchao Huang, Cheng Li, Yinxiang Zeng, Wang Wang, Yao Li, Pingping Fang, Xihong Lu, and Yexiang Tong*

Due to their unique architectures and outstanding electrical properties, three dimensional graphene-based frameworks (3DGFs) have attracted extensive attention in wide fields. However, recently reported techniques always require complex processes and high cost, which severely limit their large-scale application. In this study, the massive preparation of macroscopically porous 3DGFs from the inherently inexpensive graphite paper is for the first time realized by simply combining the modified Hummer's method with freezing technique. The as-prepared 3DGFs that consist of well exfoliated, high-quality reduced graphene oxide (RGO) exhibit a mesoporous structure and superior conductivity. Such unique features enable the 3DGFs to be directly used as a supercapacitor electrode and as ideal 3D scaffolds to create PANI@3DGFs, Pd@3DGFs, and Pt@3DGFs composites, which hold great potential applications in supercapacitors and catalysts.

1. Introduction

Three-dimensional (3D) graphene-based frameworks (3DGFs) such as foams,[1–3] aerogels,[4–8] and sponges[9,10] are emerging as a new class of ultra-light and porous carbon materials because of its unique structure and fascinating properties such as interconnected macroporous structures, large surface area, low mass density, excellent electrical conductivity, and stability. Such characteristics enable them an interesting building block/scaffold for realization of multifunctional materials applied in energy-storage devices, field-effect devices, fuel cells, sensors, solar cells, and so forth.[11–22] Given their potential applications, attempts to generate high-quality 3DGFs have been made, and several methods including template-assisted growth,[1,2,23] self-assembly,[4,24] organic sol–gel reaction,[25] and LightScribe patterning technology[26,27] have been developed for preparation of 3DGFs in recent years. For instance, Chen et al. reported a template-assisted chemical vapor deposition (CVD) approach to prepare 3D graphene foams using Ni foam as template. These 3D foams obtained at 1000 °C have shown high electrical conductivity and good mechanical properties.[2,28] Similarly, 3D graphene foams have also been obtained via hydrothermal growth of graphene/GO onto Ni foam surface at 80–180 °C. Wang et al. used a graphene oxide (GO) suspension to prepare 3DGFs by a hydrothermal process with the assistance of noble-metal salt and glucose.[24] Shi and his workers also developed a hydrothermal method to fabricate 3DGFs without any additives excepted for GO suspension.[4,24] Nevertheless, there are some challenges toward the fabrication and applications of 3DGFs. First, most of the developed approaches require high production cost, high temperature, and/or complicated manipulation and instrumentations. Second, the current methods are still not satisfactory for large-scale production of 3DGFs in low cost, which severely limit the scale-up of their applications. Therefore, it still remains a significant challenge to develop facile, mild and low-cost methods for the fabrication of 3DGFs on a large scale.

In this paper, we presented a new, template-free and cost-effective approach for the large-scale fabrication of high-quality 3DGFs from commercial graphite paper (GP) at room temperature and mild conditions. Commercial GP, made by compressing a collection of exfoliated graphite flakes without a binder, have been widely used in gasketing, electromagnetic interference shielding, electrochemical applications and stress sensing due to its good conductivity, high chemical stability, high temperature resistance, and low coefficient of thermal expansion.[29,30] Moreover, as a carbon material, GP has good biocompatibility and abundantly availability at low cost (ca. \$ 10/m^2). Herein, we demonstrated for the first time that the use of commercial GP to massively prepare macroscopically porous 3DGFs by combining the modified Hummer's method with a freezing technique. Compared with recently reported strategies for producing 3D graphene, the present method has significant advantages of simpleness, time- and energy-saving, low cost and suitable for massive production. The as-prepared 3DGFs that consisted of well exfoliated, high-quality reduced graphene oxide (RGO) exhibited meso-porous structure and superior conductivity. Such these unique features enable the 3DGFs to hold great opportunities in energy storage and catalysis. For example, when directly used as a supercapacitor electrode, the 3DGFs were able to deliver a high capacitance of 331.3 F g^{-1} at 10 mV s^{-1}, which is almost 8 times of GP electrode (42.4 F g^{-1}). When used as 3D substrate to load PANI,

M. H. Yu, Y. C. Huang, C. Li, Y. X. Zeng, W. Wang, Y. Li, Dr. P. P. Fang, Dr. X. H. Lu, Prof. Y. X. Tong
MOE of the Key Laboratory of Bioinorganic and Synthetic Chemistry
KLGHEI of Environment and Energy Chemistry
School of Chemistry and Chemical Engineering
Sun Yat-Sen University
Guangzhou 510275, P. R. China
E-mail: luxh6@mail.sysu.edu.cn

DOI: 10.1002/adfm.201402964

© 2014 WILEY-VCH Verlag GmbH & Co. KGaA, Weinheim

the PANI nanorods exhibited a highest specific capacitance of 1341.3 F g^{-1} (596.1 F g^{-1} based on the mass of the whole electrode) at a current density of 0.5 A g^{-1}. Furthermore, the as-prepared 3DGFs are ideal scaffolds to create novel 3D composites such as 3D structured Pd@3DGFs and Pt@3DGFs. Pd@3DGFs and Pt@3DGFs exhibited high catalytic activity in Suzuki reaction and formaldehyde (HCHO) oxidation reaction, respectively. Thus, given the easy large-scale synthesis and all these unique properties, we believe there is a large feasibility for the future industrial preparation and application of our 3DGFs.

2. Results and Discussion

2.1. Preparation and Characterization of 3DGFs

The synthetic procedures of macroscopically porous 3DGFs are illustrated in **Figure 1**a. In brief, commercial GP was firstly cut into a certain size such as 4 cm × 4 cm (Figure 1b). Scanning electron microscopy (SEM) images reveal that the commercial GP with a very smooth surface is composed of interlaced and compact graphite sheets (Figure 1e). Then, the commercial GP was oxidized by the modified Hummer's method in a mixture of sulfuric acid, nitric acid, and potassium permanganate (Experimental Section). Interestingly, monolithic 3D GO frameworks (denoted as 3DGOFs) composed of oxygen-containing functional group were successfully obtained after exfoliated for 3 h at room temperature and freeze-dried. The as-prepared 3DGOFs could still keep as a whole with only a little graphite falling off, and the volume was substantially expanded more than 10 times compared to pristine GP during the graphite sheets exfoliating process (Figure 1c,d). Finally, hydrazine hydrate vapor was utilized to reduce 3DGOFs into 3DGFs. Besides inherently inexpensive nature, this approach is quite possible to realize much larger scale synthesis of 3DGFs by just enlarging the equipment. The 3DGFs have good compressive strength, which could sustain large-strain deformations (e.g., more than 60%) under manual compression and recover most of the material volume without structural destruction (Figure S1, Supporting Information). Such ability to maintain structural integrity upon large deformation is very essential for macroscopic material which functions reliably. Figure 1f presents the typical SEM images of the 3DGFs. In comparison to pristine GP, the thin walls of 3DGFs are almost transparent under SEM electron irradiation. Wrinkles and ripples arisen from the thin walls consisting of a few layers of graphene sheets are clearly observed on the surface of graphene, yielding a much larger surface.

Transmission electron microscopy (TEM) was further utilized to investigate the quality and microstructure of 3DGFs. Figure S2 (Supporting Information) and **Figure 2**a, b show the typical TEM and high-resolution TEM (HRTEM) images of GP and 3DGFs, respectively. Significantly, the lower contrast image of 3DGFs indicates only a few layers of graphite sheets were remained after the chemical exfoliated process. Simultaneously, selected area electron diffraction (SAED) pattern also changes from disordered diffraction spots to a single crystalline characteristic, which is associated with the high quality of graphene sheet. Magnified TEM images further revealed the well exfoliated level of the 3DGFs (Figure 2b and Supporting Information Figure S2b). Dozens layers of graphite sheets seem to seamlessly bond to each other with no void observed in the edge of GP, while only ≈2–5 layers constitute the 3DGFs. The insert lattice-resolved TEM image in Figure 2b collected at the edge of 3DGFs revealed a lattice fringe of 0.21 nm that is consistent with the d-spacing of (100) plane of the hexagonal graphite sheet.

To assess the chemical composition evolution of 3DGFs, X-ray photoelectron spectroscopy (XPS) and Raman spectra of GP and 3DGFs were measured. The XPS Survey spectra show that there are only C and O existing on their surfaces (Figure S3a), revealing the high purity of GP and 3DGFs. Figure 2c (upper) displays the core level C1s XPS spectrum of 3DGFs, which could be de-convoluted into three synthetic peaks. The main peak centered at 284.8 eV is assigned to the sp2 carbon

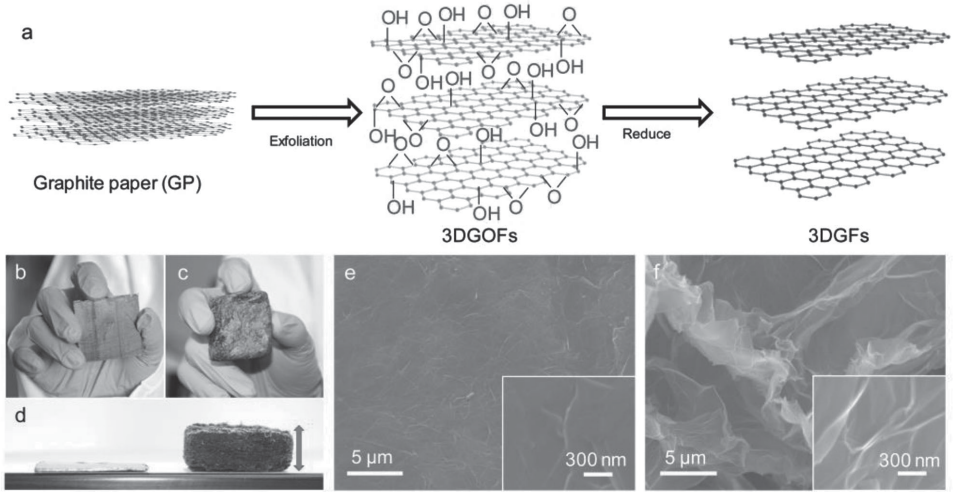

Figure 1. a) Schematic diagram illustrating the fabrication of 3DGFs. Photographs of b) GP, c) 3DGFs, and d) their comparison. SEM images of e) GP and f) 3DGFs.

© 2014 WILEY-VCH Verlag GmbH & Co. KGaA, Weinheim

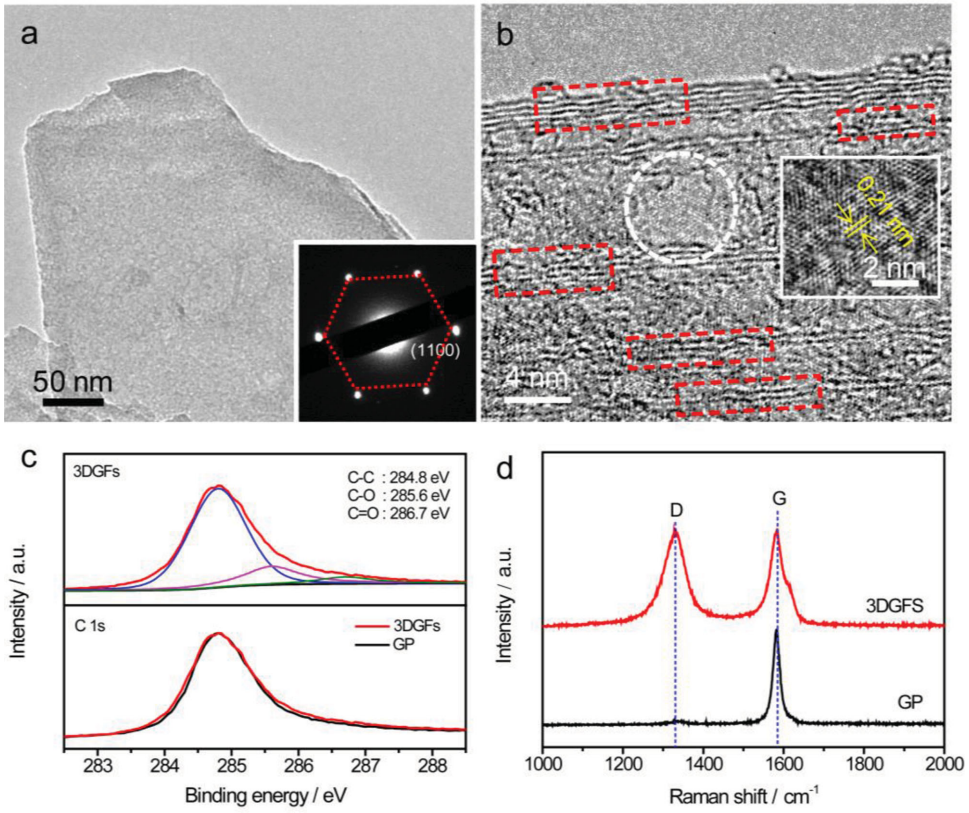

Figure 2. a) Low-magnification TEM image of 3DGFs. Inset: corresponding SAED pattern. b) High-resolution TEM image collected at the edge of 3DGFs. c) Upper: core level C 1s XPS spectrum collected for 3DGFs; Bottom: comparison of core level C 1s XPS spectra between GP and 3DGFs. d) Raman spectra collected for GP and 3DGFs.

atoms (C–C/C = C at 284.8 eV), while the weak peaks at 285.6 and 286.7 eV are associated with hydroxyl/epoxy groups (C–O) and carbonyl group (C = O), respectively.[31,32] Figure 2c (bottom) compares the core level C1s XPS spectra of GP and 3DGFs. No obvious change was observed between GP and 3DGFs, indicating that most of the epoxide and hydroxyl functional groups of the 3DGFs created in the chemical oxidation reaction were reduced. This result is further confirmed by core level O1s spectra of GP and 3DGFs that display similar shape profile (Figure S3b). Raman spectra collected for GP and 3DGFs are shown in Figure 2d. The peak located at 1329 cm^{-1} for 3DGFs matches well with the D band of graphene, which arisen from sp3 hybridized carbon.[33,34] The high I_D/I_G ratio (1:1) reveals that the 3DGFs have substantially higher edge/plane defective sites compared to the GP. Additionally, the variation of surface area during the exfoliating process was evaluated by nitrogen adsorption–desorption measurement at 77 K (Figure S4a, Supporting Information). The calculated Brunauer–Emmett–Teller (BET) surface area of 3DGFs achieved 311.8 m^2 g^{-1}, which is much larger than that of GP (58.2 m^2 g^{-1}), confirming that the surface area could be remarkably increased by this present strategy. More interestingly, our prepared 3DGFs possess higher electrical conductivity (252.0 S cm^{-1}) and faster diffusion of ions than the pristine GP (68.9 S cm^{-1}), which is confirmed by the smaller semicircle and more steeper straight line of its Nyquist plots (Figure S4b, Supporting Information). Therefore, our as-fabricated 3DGFs, combining unique porous structure and electrical properties as well as ease of scalable synthesis from inexpensive GP, hold great promise as a superior building block for constructing macroscopic three-dimensional (3D) bulk assemblies for widespread applications.

2.2. Performance of PANI@3DGFs as Supercapacitor Electrodes

Firstly, the large surface area, fast ion diffusion rate and excellent conductivity of the 3DGFs open up new opportunities to utilize our 3DGFs in energy storage application. Supercapacitors are emerging as a new class of energy storage device because they connect the gap between conventional capacitors and batteries.[35–38] Herein we evaluated the performance of 3DGFs as direct electrode and as 3D substrate of PANI@3DGFs electrode for supercapacitors. PANI nanorods were directly deposited on 3DGFs electrode through a electrodeposition method (Details please see our experimental section). As present in **Figure 3**a, uniform PANI nanorods are coated on the surface of graphene sheets. TEM images in Figure 3b show the diameters of these nanorods range from 10 to 60 nm. The electrochemical performance of GP, 3DGFs and PANI@3DGFs electrodes were examined in a three-electrode system with 1.0 M H_2SO_4 as electrolyte. **Figure 4**a displays the cyclic voltammetry (CV) curves collected for GP, 3DGFs and PANI@3DGFs electrodes at 20 mV s^{-1}. A pair of redox peaks with good symmetry, corresponding to the oxidation/reduction of residual oxygen-containing functional

© 2014 WILEY-VCH Verlag GmbH & Co. KGaA, Weinheim

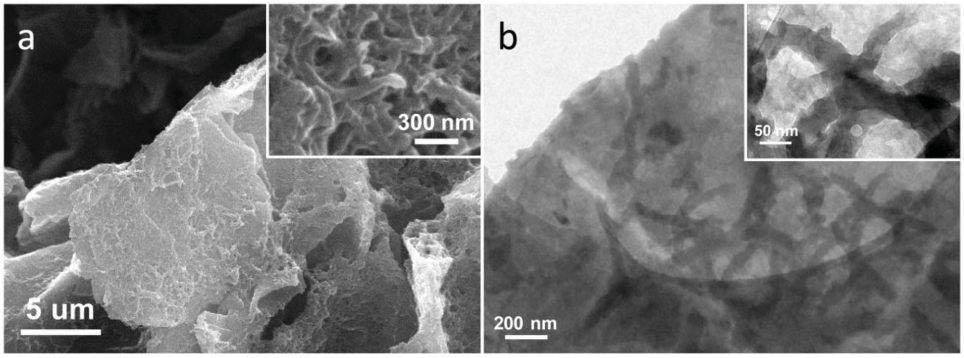

Figure 3. a) SEM and b) TEM images of PANI@3DGFs.

groups,[39,40] was clearly observed for both the GP and 3DGFs electrodes, revealing that they have pseudocapacitive characteristics. In comparison with GP electrode, substantially increased area of the CV curve by more than one order of magnitude was achieved by 3DGFs electrode, indicating the 3DGFs electrode own considerably improved charge-storage capabilities. As expected, by introducing pseudocapacitive behavior of PANI into composite electrode, the area of the CV curve was further enlarged when compared with that of 3DGFs electrodes. CV curves of GP, 3DGFs and PANI@3DGFs electrodes at different scan rates are shown in Figure S5 (Supporting Information). The maximum specific capacitance of 3DGFs electrode reached 331.3 F g^{-1} at 10 mV s^{-1}, which is almost 8 times of GP electrode (42.4 F g^{-1}). Noteworthy is that, despite of the porous and loosen structure, the 3DGFs still possess a high volumetric capacitance of 3.1 F cm^{-3} at 10 mV s^{-1}, which is substantially higher or comparable with recently reported bulk carbon based electrode.[41–46] Besides, Figure 4b summarizes the calculated capacitance of PANI@3DGFs electrode at different scan rates. As can be observed, the specific capacitance of PANI@3DGFs electrode was extended into 931.8 F g^{-1} at 10 mV s^{-1} (based on the mass of the whole electrode), which is more than 4 times of pristine 3DGFs electrode. Impressively, the specific capacitance based on the mass of PANI reached 1681.2 F g^{-1}.

Galvanostatic charge/discharge measurements were further utilized to evaluate the electrochemical performance of PANI@3DGFs electrode. Figure 4c shows the galvanostatic charge/discharge curves at different currents. Relatively symmetric profiles indicate its rapid charge/discharge property and reversible pseudocapacitive behavior. Corresponding

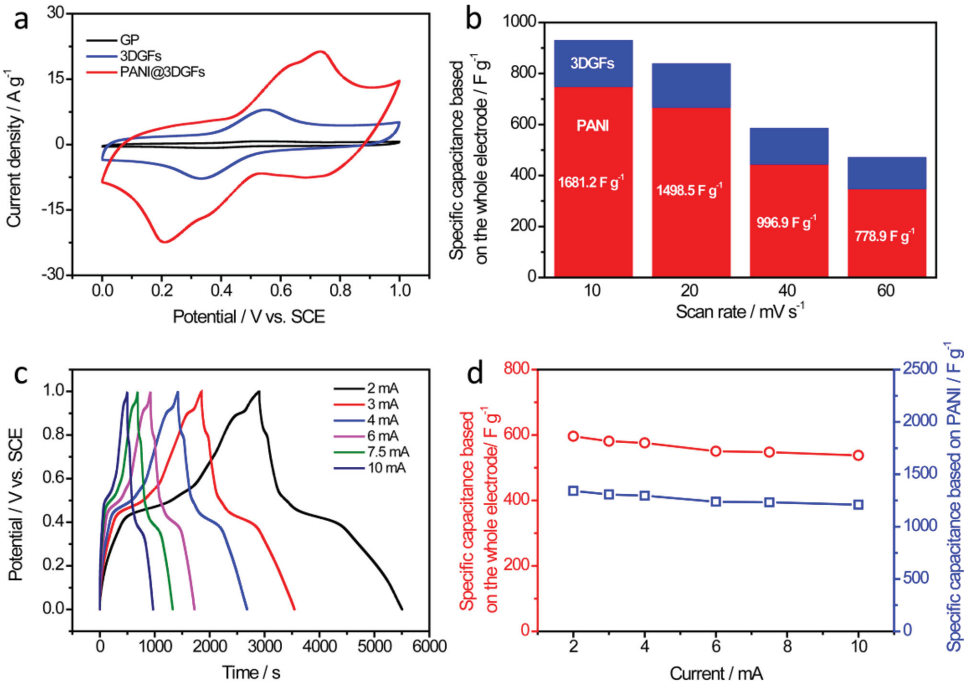

Figure 4. a) CV curves collected at 20 mV s^{-1} of GP, 3DGFs and PANI@3DGFs electrodes. b) Histogram illustration of capacitance contribution from 3DGFs substrate and PANI for PANI@3DGFs electrodes at different scan rates. c) Galvanostatic charge/discharge curves of PANI@3DGFs electrode collected at various current. d) Specific capacitance based on the mass of the whole electrode and PANI calculated for PANI@3DGFs electrode based on the galvanostatic charge/discharge curves as a function of current.

© 2014 WILEY-VCH Verlag GmbH & Co. KGaA, Weinheim

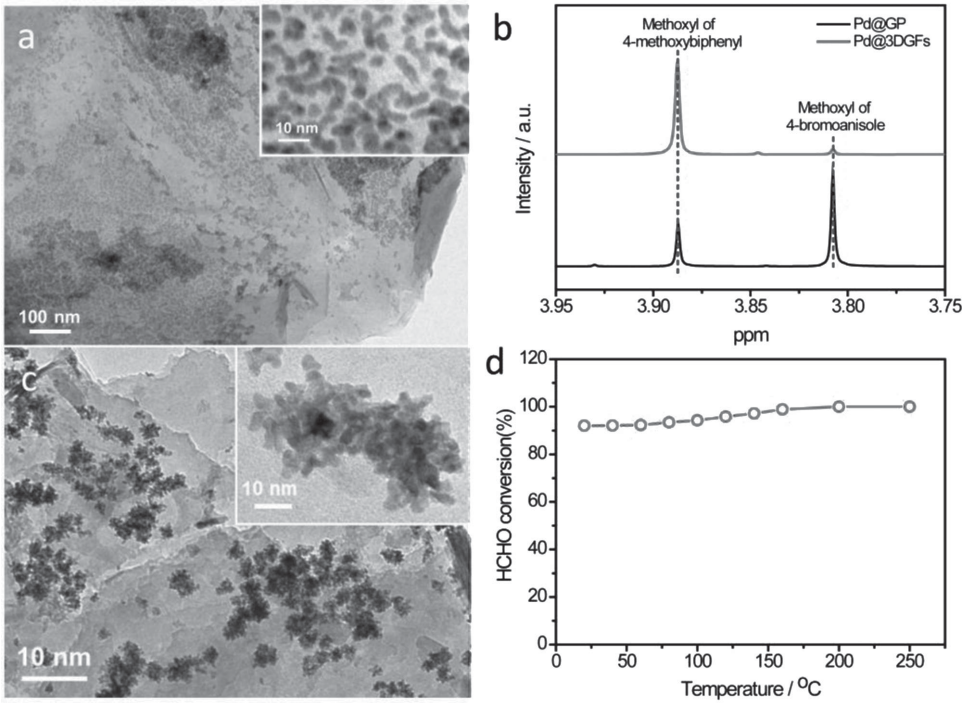

Figure 5. a) TEM images of Pd@3DGFs. b) ^{1}H nuclear magnetic resonance (NMR) spectra of the Suzuki reaction mixture after 1 h reaction time catalyzed by Pd@3DGFs and Pd@GP. c) TEM of Pt@3DGFs. d) Formaldehyde catalytic performance of Pt@3DGFs.

specific capacitances based on the mass of the whole electrode and PANI calculated for PANI@3DGFs electrode are shown in Figure 4d. The PANI nanorods exhibited a highest specific capacitance of 1341.3 F g^{-1} (596.1 F g^{-1} based on the mass of the whole electrode) at a current of 2 mA (current density considering the mass of PANI: 0.5 A g^{-1}), which is considerably higher than the values in recent reports for PANI electrodes, such as PANI film[47] (214 F g^{-1} at 0.3 A g^{-1}), PANI/RGO[48] (480 F g^{-1} at 0.1 A g^{-1}), PANI@carbon cloth[49] (1079 F g^{-1} at 1.73 A g^{-1}), PANI/CNT[50] (400 F g^{-1} at 0.1 A g^{-1}), PANI/curved RGO[51] (553 F g^{-1} at 1 A g^{-1}). Significantly, when the current increased into 10 mA, the specific capacitance still remained 1209.7 F g^{-1} (537.6 F g^{-1} based on the mass of the whole electrode) with 90.2% capacitance retention. We also studied the long-term cycling stability of PANI@3DGFs electrode at a scan rate of 40 mV s^{-1}. As shown in Figure S6 (Supporting Information), PANI@3DGFs electrode possessed a normal electrochemical stability of 70.2% capacitance retention after 5000 cycles, which is comparable with that of recently reported PANI based electrodes.[47,49,52–54] The remarkable capacitance decay in the first 500 cycles is believed to be due to the structural breakdown of PANI as a result of ion doping and de-doping during repeated charging and discharging processes.[50,55,56] This volumetric alternation lead the precarious PANI of the surface to structural breakdown and falling off from the main structure. After this process, a relatively stable structure gradually come into being for PANI main structure, and thus retained relatively stable cycling performance after 500 cycles. All these excellent performances of 3DGFs electrode can be ascribed to the following reasons: First, the interlaced morphology of PANI and highly conductive nature of graphene enables rapid charge transport via the network. Second, the 3D graphene network consisting of numerous meso pore guarantees the large surface area, resulting in fast and easy access of electrolyte ions to the surface of electrode. Third, the direct connection between electrochemically active PANI nanorods with 3DGFs substrate can effectively facilitate the interfacial charge transfer.

2.3. Performance of Pd@3DGFs and Pt@3DGFs as Catalysis

On the other hand, as efficient catalysts, noble metals have been widely used in electrocatalysis and organic synthesis. Forming nano-sized noble metals can efficiently increase their surface area and active sites, hence resulting in higher catalytic efficiency and lower cost. Herein, we further loaded palladium (Pd) nanoparticle on 3DGFs. It can be seen Pd nanoparticles with diameter of 2–10 nm are scattered on the surface of 3DGFs from TEM images (**Figure 5**a) and SEM images (Figure S7, Supporting Information). The catalytic activity of as-fabricated Pd@3DGFs was explored using Suzuki reaction of 4-bromoanisole with phenylboronic acid in water with base of K_2CO_3 (Schematic representation of the Suzuki reaction under aqueous conditions is as shown in Figure S7c, detailed reaction condition is described in experimental section). Pd@GP catalyst was also fabricated to make comparison. Figure 5b presents the ^{1}H nuclear magnetic resonance (NMR) information of the reaction mixture after 1 h reaction time using Pd@3DGFs and Pd@GP as catalyst (both 2 mol% Pd), respectively. The peaks located at 3.887 ppm correspond to the methoxyl of 4-methoxybiphenyl, while the peaks at 3.807 ppm is in consistent with the methoxyl of 4-bromoanisole. It can be concluded that traces of

© 2014 WILEY-VCH Verlag GmbH & Co. KGaA, Weinheim

reactant exist in the Pd@3DGFs system after only 1 h reaction. The calculated yield through the area ratio of these two kinds of methoxyl peaks is up to 95.1%, which is much higher than the yield in Pd@GP system (only 31.8%), suggesting the excellent catalytic property of Pd@3DGFs. Finally, nano-sized platinum (Pt) was successfully synthesized on 3DGFs. Similar morphology with Pd@3DGFs was confirmed for Pt@3DGFs, while the diameters ranged from 2 to 5 nm (Figure 5c). Such as-fabricated Pt@3DGFs catalyst exhibited a high catalytic activity in HCHO oxidation, showing a large HCHO conversion of 92.0% even at room temperature (Figure 5d, detailed reaction condition can be seen in experimental section). All these results demonstrated the feasibility of 3DGFs as ideal scaffolds.

3. Conclusion

In summary, we have developed a template-free and cost-effective method for the massively fabrication of high-quality 3DGFs from GP under mild conditions. By combining the modified Hummer's method with freezing technique, the as-prepared 3DGFs expressed a huge volume expansion of more than 10 times compared to pristine GP, meanwhile the specific surface area was increased by more than 3 times. Besides, 3DGFs also exhibited a superior conductivity due to multiple efficiency conductive pathways provided by its 3D structure. Simultaneously, this method is quite possible to realize larger scale synthesis by enlarging the device. We believe that such an inherently inexpensive, scalable, facile method can significantly increase the feasibility of future industrial preparation. Additionally, the successful synthesis of 3DGFs further pave the way to explore the application of graphene in a self-supporting, structurally adaptive and 3D macroscopic form. Herein, we have demonstrated the direct use of 3DGFs as capacitive electrode with high performance and as versatile 3D scaffolds to create PANI@3DGFs, Pd@3DGFs and Pt@3DGFs composites, which should find applications in 3D electrode materials for supercapacitors and catalyst.

4. Experimental Section

Fabrication of 3DGFs: 3DGFs were prepared by oxidation of GP according to the modified Hummers's method. Briefly, a piece of GP (4 cm × 4 cm, 2 g) was immerged in a solution containing concentrated sulfuric acid (40 mL) and concentrated nitric acid (10 mL). The mixture was cooled down to 0 °C. Then $KMnO_4$ (6 g) was slowly added to the mixture, and the reaction system was transferred to keep at 35 °C for 3 h. Successively, distilled water (200 mL) was added, and followed by dropwise adding H_2O_2 solution (30 wt%) until no gas bubbles evolved. The treated GP was then washed with HCl solustion (10 wt%) and distiled water, and freeze-dried. Finally, the treated GP was reduced by hydrazine vapor. In details, the treated GP was placed in a 100 mL sealed container, which contained hydrazine (2 mL). Then the container was heated at 85 °C for 24 h.

Fabrication of PANI@3DGFs: PANI was electrodeposited on the 3DGFs (0.5 cm × 1 cm × 1 cm) using cyclic voltammetry technique in a simple three-electrode cell with an electrochemical workstation (CHI 760E). A Pt wire was used as counter electrode, while a saturated calomel electrode was used as reference electrode. The electolyte in this reaction was a solution of 0.1 M aniline and 1 M H_2SO_4. And the detailed parameter of cyclic voltammetry method is: potential range: 0–1 V, scan rate 10 mV s^{-1}, 2 cycles. 9 mg PANI@3DGFs contains 4 mg PANI.

Fabrication of Pd@3DGFs and Pd@GP: Pd@3DGFs were prepared at room temperature by a combined NaOH assisted impregnation of 3DGFs with Pd precursor and $NaBH_4$ reduction process. Typically, 3DGFs (15 mg, 0.1 cm^3) was added in to H_2PdCl_4 (5 mL, 10 mM) solution. After impregnation for 6 h, 2.5 mL of the mixed solution of $NaBH_4$ solution (0.1 M) and NaOH solution (0.5 M) were quickly added into the suspension. After another 6 h, the 3DGFs were taken out and washed by distilled. Finally, the 3DGFs were freeze-dried again. For comparison, the same synthesis process was conducted for GP (120 mg, 0.1 cm^3) under same condition.

Fabrication of Pt@3DGFs: Pt@3DGFs were also prepared at room temperature by a combined NaOH assisted impregnation of 3DGFs with Pd precursor and $NaBH_4$ reduction process. 3DGFs (15 mg, 0.1 cm^3) was added in to H_2PtCl_6 (5 mL, 10 mM) solution. After impregnation for 6 h, 2.5 mL of the mixed solution of $NaBH_4$ solution (0.1 M) and NaOH solution (0.5 M) were quickly added into the suspension. After another 6 h, the 3DGFs were taken out and washed by distilled. Finally, the 3DGFs were freeze-dried again.

Suzuki Reaction Catalyzed by Pd@3DGFs: A mixture of K_2CO_3 (1.5 mmol), phenylboronic acid (0.75 mmol) and deionized water (25 mL) was taken in a 250 mL round bottom flask. 4-bromoanisole (0.5 mmol) was added into the mixture under stirring, followed by the addition of as-fabricated Pd@3DGFs (total mass 30 mg, Pd 2 mol%). After stirred at 60 °C in a water bath for 1 h, the reaction mixture was extracted thrice with diethyl ether (30 mL), then washed twice with deionized water (30 mL). Finally the ^1H NMR was used to determine the yield. For comparison, the same reaction catalyzed by Pd@GP was conducted under same condition.

HCHO Oxidation Reaction Catalyzed by Pt@3DGFs: The HCHO oxidation reaction was performed in a fixed-bed reactor under atmospheric pressure with the catalyst (200 mg, 40–60 mesh, Pt: 2 wt%) loaded in a quartz tube reactor. The HCHO-containing stream was generated by passing a purified air flow (N_2/O_2 = 4, 100 mL/min) over HCHO solution in an incubator kept at 0 °C, leading to a feed gas with 50 ppm of HCHO. The gas hourly space velocity (GHSV) is 30 000 mL h^{-1} g^{-1}. HCHO concentration in the reactant or product gas stream was analyzed by phenol spectrophotometric method. The gas stream containing trace HCHO was bubbled through 5 mL phenol reagent($C_6H_4SN(CH_3)C$: NNH_2·HCl, Alfa Aesar) solution (1×10^{-4} wt%) for 30 s to collect HCHO. Then, 0.4 mL (1 wt%) ammonium ferric sulfate ($NH_4Fe(SO_4)_2.12H_2O$, Tianjin Fuchen Chemical Reagent Company) solution was added as the coloring reagent. After shaking for 5 s and staying for 15 min in the dark, HCHO concentration in the gas stream was then determined by measuring light absorbance at 630 nm with a spectrophotometer (UV-240, Shimadzu Co. Ltd., Japan). The conversion of HCHO was calculated based on its concentration change.

Material Characterization and Electrochemical Measurement: The microstructures and compositions of electrode materials were analyzed by field-emission SEM (FE-SEM, JSM-6330F), Raman spectroscopy (Renishaw inVia) and XPS (XPS, ESCALab250, Thermo VG). Conductivities of our samples were measured by a standard four-probe method using a physical property measurement system (ST2253). Cyclic voltammetry (CV), galvanostatic charge/discharge measurements and electrochemical impedance electrochemical workstation (CHI 760E). The electrochemical studies of GP and 3DGFs electrodes were performed in a conventional three-electrode cell, using a Pt counter electrode and a saturated calomel reference electrode (SCE) in 1 M H_2SO_4 aqueous solution.

Supporting Information

Supporting Information is available from the Wiley Online Library or from the author.

© 2014 WILEY-VCH Verlag GmbH & Co. KGaA, Weinheim

Acknowledgements

The authors acknowledge the financial support of this work by the Natural Science Foundations of China (21273290 and 91323101), Natural Science Foundations of Guangdong Province (S2013030013474), the Research Fund for the Doctoral Program of Higher Education of China (20120171110043) and the National Undergraduates Innovating Experimentation Project.

Received: August 27, 2014
Revised: October 4, 2014
Published online: November 20, 2014

[1] X. Cao, Y. Shi, W. Shi, G. Lu, X. Huang, Q. Yan, Q. Zhang, H. Zhang, *Small* **2011**, *7*, 3163.
[2] Z. Chen, W. Ren, L. Gao, B. Liu, S. Pei, H. M. Cheng, *Nat. Mater.* **2011**, *10*, 424.
[3] W. Wei, S. Yang, H. Zhou, I. Lieberwirth, X. Feng, K. Mullen, *Adv. Mater.* **2013**, *25*, 2909.
[4] Y. Xu, K. Sheng, C. Li, G. Shi, *ACS Nano* **2010**, *4*, 4324.
[5] H. Bi, K. Yin, X. Xie, Y. Zhou, N. Wan, F. Xu, F. Banhart, L. Sun, R. S. Ruoff, *Adv. Mater.* **2012**, *24*, 5124.
[6] K. H. Kim, Y. Oh, M. F. Islam, *Nat. Nanotechnol.* **2012**, *7*, 562.
[7] H. W. Liang, Q. F. Guan, L. F. Chen, Z. Zhu, W. J. Zhang, S. H. Yu, *Angew. Chem. Int. Ed.* **2012**, *51*, 5101.
[8] Y. Tao, M. Endo, K. Kaneko, *J. Am. Chem. Soc.* **2009**, *131*, 904.
[9] H. W. Liang, Q. F. Guan, Z. Zhu, L. T. Song, H. B. Yao, X. Lei, S. H. Yu, *NPG Asia Mater.* **2012**, *4*, e19.
[10] H. B. Yao, J. Ge, C. F. Wang, X. Wang, W. Hu, Z. J. Zheng, Y. Ni, S. H. Yu, *Adv. Mater.* **2013**, *25*, 6692.
[11] W. Zhou, J. Zhu, C. Cheng, J. Liu, H. Yang, C. Cong, C. Guan, X. Jia, H. J. Fan, Q. Yan, C. M. Li, T. Yu, *Energy Environ. Sci.* **2011**, *4*, 4954.
[12] C. Wu, J. Feng, L. Peng, Y. Ni, H. Liang, L. He, Y. Xie, *J. Mater. Chem.* **2011**, *21*, 18584.
[13] J. Luo, J. Liu, Z. Zeng, C. F. Ng, L. Ma, H. Zhang, J. Lin, Z. Shen, H. J. Fan, *Nano Lett.* **2013**, *13*, 6136.
[14] L. Peng, X. Peng, B. Liu, C. Wu, Y. Xie, G. Yu, *Nano Lett.* **2013**, *13*, 2151.
[15] H. Zhu, Z. Fang, C. Preston, Y. Li, L. Hu, *Energy Environ. Sci.* **2014**, *7*, 269.
[16] K. S. Novoselov, A. K. Geim, S. V. Morozov, D. Jiang, Y. Zhang, S. V. Dubonos, I. V. Grigorieva, A. A. Firsov, *Science* **2004**, *306*, 666.
[17] T. Maiyalagan, X. Dong, P. Chen, X. Wang, *J. Mater. Chem.* **2012**, *22*, 5286.
[18] H. Bi, F. Huang, J. Liang, Y. Tang, X. Lü, X. Xie, M. Jiang, *J. Mater. Chem.* **2011**, *21*, 17366.
[19] X. C. Dong, H. Xu, X. W. Wang, Y. X. Huang, M. B. Chan-Park, H. Zhang, L. H. Wang, W. Huang, P. Chen, *ACS Nano* **2012**, *6*, 3206.
[20] Y. Yang, G. Ruan, C. Xiang, G. Wang, J. M. Tour, *J. Am. Chem. Soc.* **2014**, *136*, 6187.
[21] C. Biswas, Y. H. Lee, *Adv. Funct. Mater.* **2011**, *21*, 3806.
[22] H. Chang, H. Wu, *Adv. Funct. Mater.* **2013**, *23*, 1984.
[23] L. Estevez, A. Kelarakis, Q. Gong, E. H. Da'as, E. P. Giannelis, *J. Am. Chem. Soc.* **2011**, *133*, 6122.
[24] Z. Tang, S. Shen, J. Zhuang, X. Wang, *Angew. Chem. Int. Ed.* **2010**, *49*, 4603.
[25] M. A. Worsley, P. J. Pauzauskie, T. Y. Olson, J. Biener, J. H. Satcher, T. F. Baumann, *J. Am. Chem. Soc.* **2010**, *132*, 14067.
[26] M. F. El-Kady, V. Strong, S. Dubin, R. B. Kaner, *Science* **2012**, *335*, 1326.
[27] V. Strong, S. Dubin, M. F. El-Kady, A. Lech, Y. Wang, B. H. Weiller, R. B. Kaner, *ACS Nano* **2012**, *6*, 1395.
[28] W. Chen, S. Li, C. Chen, L. Yan, *Adv. Mater.* **2011**, *23*, 5679.
[29] R. Chugh, D. D. L. Chung, *Carbon* **2002**, *40*, 2285.
[30] J. Chen, K. Li, Y. Luo, X. Guo, D. Li, M. Deng, S. Huang, Q. Meng, *Carbon* **2009**, *47*, 2704.
[31] A. J. Patil, J. L. Vickery, T. B. Scott, S. Mann, *Adv. Mater.* **2009**, *21*, 3159.
[32] L. Tang, Y. Wang, Y. Li, H. Feng, J. Lu, J. Li, *Adv. Funct. Mater.* **2009**, *19*, 2782.
[33] U. N. Maiti, J. Lim, K. E. Lee, W. J. Lee, S. O. Kim, *Adv. Mater.* **2014**, *26*, 615.
[34] J. Yan, Z. Fan, W. Sun, G. Ning, T. Wei, Q. Zhang, R. Zhang, L. Zhi, F. Wei, *Adv. Funct. Mater.* **2012**, *22*, 2632.
[35] Z. Yu, B. Duong, D. Abbitt, J. Thomas, *Adv. Mater.* **2013**, *25*, 3302.
[36] Z. Yu, J. Thomas, *Adv. Mater.* **2014**, *26*, 4279.
[37] Y. Meng, K. Wang, Y. Zhang, Z. Wei, *Adv. Mater.* **2013**, *25*, 6985.
[38] J. Xu, K. Wang, S. Z. Zu, B. H. Han, Z. Wei, *ACS Nano* **2010**, *4*, 5019.
[39] Y. Shao, J. Wang, M. Engelhard, C. Wang, Y. Lin, *J. Mater. Chem.* **2010**, *20*, 743.
[40] Y. Chen, X. Zhang, D. Zhang, P. Yu, Y. Ma, *Carbon* **2011**, *49*, 573.
[41] T. Zhai, F. Wang, M. Yu, S. Xie, C. Liang, C. Li, F. Xiao, R. Tang, Q. Wu, X. Lu, Y. Tong, *Nanoscale* **2013**, *5*, 6790.
[42] W. Gao, N. Singh, L. Song, Z. Liu, A. L. Reddy, L. Ci, R. Vajtai, Q. Zhang, B. Wei, P. M. Ajayan, *Nat. Nanotechnol.* **2011**, *6*, 496.
[43] C. Emmenegger, P. Mauron, P. Sudan, P. Wenger, V. Hermann, R. Gallay, A. Züttel, *J. Power Sources* **2003**, *124*, 321.
[44] Z. Niu, J. Chen, H. H. Hng, J. Ma, X. Chen, *Adv. Mater.* **2012**, *24*, 4144.
[45] D. N. Futaba, K. Hata, T. Yamada, T. Hiraoka, Y. Hayamizu, Y. Kakudate, O. Tanaike, H. Hatori, M. Yumura, S. Iijima, *Nat. Mater.* **2006**, *5*, 987.
[46] Y. Zhao, C. Hu, Y. Hu, H. Cheng, G. Shi, L. Qu, *Angew. Chem. Int. Ed.* **2012**, *124*, 11533.
[47] Q. Wu, Y. Xu, Z. Yao, A. Liu, G. Shi, *ACS Nano* **2010**, *4*, 1963.
[48] K. Zhang, L. L. Zhang, X. S. Zhao, J. Wu, *Chem. Mater.* **2010**, *22*, 1392.
[49] Y. Y. Horng, Y. C. Lu, Y. K. Hsu, C. C. Chen, L. C. Chen, K. H. Chen, *J. Power Sources* **2010**, *195*, 4418.
[50] C. Meng, C. Liu, L. Chen, C. Hu, S. Fan, *Nano Lett.* **2010**, *10*, 4025.
[51] W. Chen, R. B. Rakhi, H. N. Alshareef, *Nanoscale* **2013**, *5*, 4134.
[52] X. Yan, Z. Tai, J. Chen, Q. Xue, *Nanoscale* **2011**, *3*, 212.
[53] H. Wang, Q. Hao, X. Yang, L. Lu, X. Wang, *Nanoscale* **2010**, *2*, 2164.
[54] L. Zheng, Y. Wang, X. Wang, N. Li, H. An, H. Chen, J. Guo, *J. Power Sources* **2010**, *195*, 1747.
[55] T. Liu, L. Finn, M. Yu, H. Wang, T. Zhai, X. Lu, Y. Tong, Y. Li, *Nano Lett.* **2014**, *14*, 2522.
[56] Y. Zhao, B. R. Liu, L. J. Pan, G. H. Yu, *Energy Environ. Sci.* **2013**, *6*, 2856.

© 2014 WILEY-VCH Verlag GmbH & Co. KGaA, Weinheim